ELSEVIER

Earth and Planetary Science Letters 183 (2000) 161–177

EPSL

www.elsevier.com/locate/epsl

Geomagnetic paleointensity and environmental record from Labrador Sea core MD95-2024: global marine sediment and ice core chronostratigraphy for the last 110 kyr

J.S. Stoner [a,*], J.E.T. Channell [b], C. Hillaire-Marcel [c], C. Kissel [d]

[a] *Department of Geology, University of California at Davis, Davis, CA 95616, USA*
[b] *Department of Geological Sciences, University of Florida, Gainesville, FL 32611-2120, USA*
[c] *GEOTOP, Université de Québec a Montréal, Montreal, Que., Canada, H3C 3P8*
[d] *Laboratoire des Sciences du Climat et de l'Environnement, 91198 Gif-sur-Yvette, France*

Received 8 May 2000; received in revised form 13 September 2000; accepted 15 September 2000

Abstract

Piston core MD95-2024 from the Labrador Rise provides a continuous record of rapidly deposited detrital layers denoting Laurentide ice sheet (LIS) instability. The core also provides a high-resolution record of geomagnetic paleointensity, that is consistent with, but at higher temporal resolution than previous Labrador Sea records. Correlation to the Greenland Summit ice cores (GRIP/GISP2) is achieved by assuming that Labrador Sea detrital layers correspond to cold stadials in the ice cores. This allows a GISP2 official chronology to be placed on MD95-2024 which is consistent with the inverse correlation between paleointensity and the flux of cosmogenic isotopes (^{10}Be and ^{36}Cl) in Greenland ice cores. Synchronous millennial scale variability observed from the MD95-2024 paleointensity record and a North Atlantic paleointensity stack (NAPIS-75) [C. Laj et al., Philos. Trans. R. Soc. Ser. A 358 (2000) 1009–1025], independently placed on the GISP2 official chronology [C. Kissel et al., Earth Planet. Sci. Lett. 171 (1999) 489–502], further support the sediment to ice core correlation. High-resolution paleointensity and oxygen isotope records from the North Atlantic, Mediterranean, Somali Basin, sub-Antarctic South Atlantic and the relative flux of ^{10}Be in Vostok (Antarctic) ice core are used to derive a common chronostratigraphy that neither violates the regional (millennial) or global (orbital) scale environmental stratigraphics. The resulting correlation circuit places the ice core and marine records on a common GISP2 official chronology, which indicates discrepancies as high as 5 kyr between the GISP2 and SPECMAP time scales. It further demonstrates that LIS instabilities in the Hudson Strait area are synchronous with cooling in the Greenland Summit ice cores and warming in the sub-Antarctic South Atlantic and in the Vostok ice core. Geomagnetic field intensity shows common global variance at millennial time scales which, in view of the out-of-phase interhemispheric climate variability, cannot be attributed to climatic contamination of the paleointensity records.

Keywords: paleomagnetism; magnetic intensity; Holocene; chronostratigraphy; climate change; Labrador Sea; ice cores

1. Introduction

High-resolution proxy records of geomagnetic paleointensity from the Labrador Sea [3,4], the

* Corresponding author. Tel.: +1-530-752-1861; Fax: +1-530-752-0951; E-mail: stoner@geology.ucdavis.edu

0012-821X/00/$ – see front matter
PII: S0012-821X(00)00272-7

North Atlantic [1,5], the Mediterranean [6], the Somali Basin [7], and the sub-Antarctic South Atlantic [8] display high-frequency variability that can be correlated to the millennial level [1,3,8]. Long period (>10 kyr) global variability of the geomagnetic paleointensity record for the last 200 kyr is now well established and tied to the SPECMAP $\delta^{18}O$ record [9]. A new millennial scale correlation of paleointensity records from different ocean basins was developed for the 10–75 ka interval using a high-resolution paleointensity stack from North Atlantic (NAPIS-75) independently tied to the Greenland Summit ice core (GISP2) official chronology [1].

Here we report a new paleointensity record from a Labrador Sea piston core, that clearly records high-frequency detrital layers derived from Laurentide ice sheet (LIS) instabilities. The relative position of these LIS events provide an independent tool for transferring the Labrador Sea paleointensity record on to the GISP2 official chronology. We assess the global resolution of the paleointensity record through high-resolution millennial scale paleoclimatic and environmental stratigraphies, global scale orbital stratigraphies, interhemispheric synchronization provided by trapped gas within Arctic and Antarctic ice cores, and the inverse relationship between geomagnetic field intensity and the production of cosmogenic isotopes.

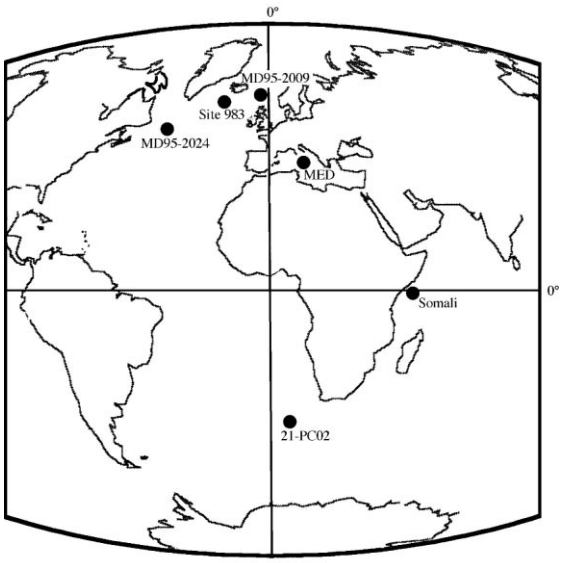

Fig. 1. Location map showing the position of paleointensity records discussed in this study. MD95-2024 (this study), MD95-2009 [1], ODP Site 983 [5], Mediterranean Stack (MED) [6], Somali Basin Stack (Somali) [7] and TTN-057-21-PC02 (21-PC02) [8].

2. Core MD95-2024 (Labrador Sea)

Labrador Sea core MD95-2024 (latitude/longitude: 50°12.26N/45°41.14W, water depth 3448 m) (Fig. 1) is a 27.34 m long piston core collected by the R.V. *Marion Dufresne II* from the Labrador Rise in a small channel east of Orphan Knoll near the location of core HU91-045-094 (P-094) [3,4,10]. Core P-094 provided a marine record of LIS instability in the form of rapidly deposited detrital layers intercalated in background hemipelagic sediments [10,11]. Correlation of the Labrador Sea paleointensity stack, which included P-094, to the Sint-200 paleointensity composite [9], allowed a SPECMAP consistent chronology to be placed on the Labrador Sea sediments and an unambiguous correlation of Labrador Sea detrital layers to North Atlantic Heinrich and higher frequency IRD events [4].

In view of the detailed work on P-094, an initial stratigraphy for MD95-2024 is provided by the correlation of common lithologic features between the two cores. The lithologic ties are conveniently recognized by comparison of magnetic parameters such as low field volumetric magnetic susceptibility (k) ($r=0.745$) and k_{ARM}/k ($r=0.915$), a magnetite grain size proxy (see [10]). The correlation indicates that the mean sedimentation rate for MD95-2024 (22 cm/kyr) is approximately twice that of P-094. Post-cruise analysis suggests that upper sections of several cores taken during the 1995 IMAGES campaign were stretched during coring, however, the similarity between the P-094 and MD95-2024 records indicate no apparent distortion of the physical properties. Except for two short intervals (1210–1252 and 1285–1330 cm) that could not be sampled due to sediment deformation, caused by a crack in the core liner, no other sediment disturbance has been observed

although the integrity of the Holocene section in this core has been questioned.

Planktic $\delta^{18}O$ data from MD95-2024 were derived from *Neogloboquadrina pachyderma* (sin.) selected from the 125–250 μm size fraction sampled at 5 cm intervals. CO_2 was extracted at 90°C using an ISOCARB device on-line with a VG-PRISM mass spectrometer with an overall analytical uncertainty of ± 0.05‰ ($\pm 1\sigma$) at Université de Québec a Montréal (see [12]). Note that *N. pachyderma* (sin.) shells in the 125–250 μm size range show a -0.38‰ offset in their $\delta^{18}O$ values when compared with the 150–250 μm size fraction [12]. The paucity of benthos precluded a continuous benthic isotope record, and the influence of meltwater on the planktic $\delta^{18}O$ compromises the record for precise chronological determinations. The SPECMAP consistent chronostratigraphy for the Labrador Sea [4], based on paleointensity correlations, has been transferred to MD95-2024 based on lithologic correlation to P-094 (**EPSL Online Background Dataset**, Fig. 1[1]).

3. Magnetic measurements

3.1. Sampling and measurement procedure

Magnetic data were acquired from u-channel samples measured on a 2G Enterprises high-resolution cryogenic magnetometer at Gif-sur-Yvette, France [13]. U-channel samples are collected by pushing rigid u-shaped plastic liners (2×2 cm cross-section), up to 150 cm in length, into the archive halves of core sections. Magnetic measurements on u-channel samples were made at 1 cm intervals, however, the width at half-height of the response function of the magnetometer pick-up coils (4.5 cm) [13] is such that adjacent measurements at 1 cm spacing are not independent and the data are therefore smoothed. This slight smoothing with respect to discrete sample measurements (for core P-094) is partially offset by the decrease in sediment deformation during u-channel sampling and the significantly greater speed with which the measurements can be made.

The following magnetic measurements were made at 1 cm intervals on u-channel samples from MD95-2024. Natural remanent magnetization (NRM) was measured and stepwise demagnetized using peak alternating fields (AF) of 10, 25, 35 and 45 mT (Fig. 2). Anhysteretic remanent magnetization (ARM) was then imposed using a 100 mT peak AF and a 0.05 mT direct current (dc) biasing field. The ARM was measured after AF demagnetization at peak fields of 25, 35 and 45 mT (Fig. 2). Isothermal remanent magnetization (IRM) was produced in a steady dc field of 0.5 T and AF demagnetized at peak fields of 25, 35 and 45 mT (Fig. 2). Measurements of k were made at 1 cm intervals using a vertical translation system with a spatial resolution of approximately 5 cm (Fig. 2).

3.2. Directional magnetic data

NRM component directions were calculated (at 1 cm intervals) using the standard least squares method [14] applied to the 10–45 mT demagnetization interval. Component inclinations, declinations and maximum angular deviation (MAD) values are shown in Fig. 3. All MAD values are below 10° and generally less than 3° indicating that the magnetization components are well defined. The inclination varies about mean values close to the expected inclination (67°) for the site latitude. The declinations are variable as expected at this high latitude, but also show some clear deviations within detrital layers that may be related to twisting of sediment during the coring of these coarser grained layers.

3.3. Paleointensity determinations

The intensity of the NRM of a sediment depends on the intensity of the geomagnetic field and the mineralogy, grain size and concentration of the magnetic remanence carriers. If the magnetic carrier is single domain or pseudo-single domain magnetite, then a laboratory induced magnetization such as IRM or ARM can be used to normalize the NRM for changes in concentration

[1] http://www.elsevier.nl/locate/espl, mirror site: http://www.elsevier.com/locate.espl

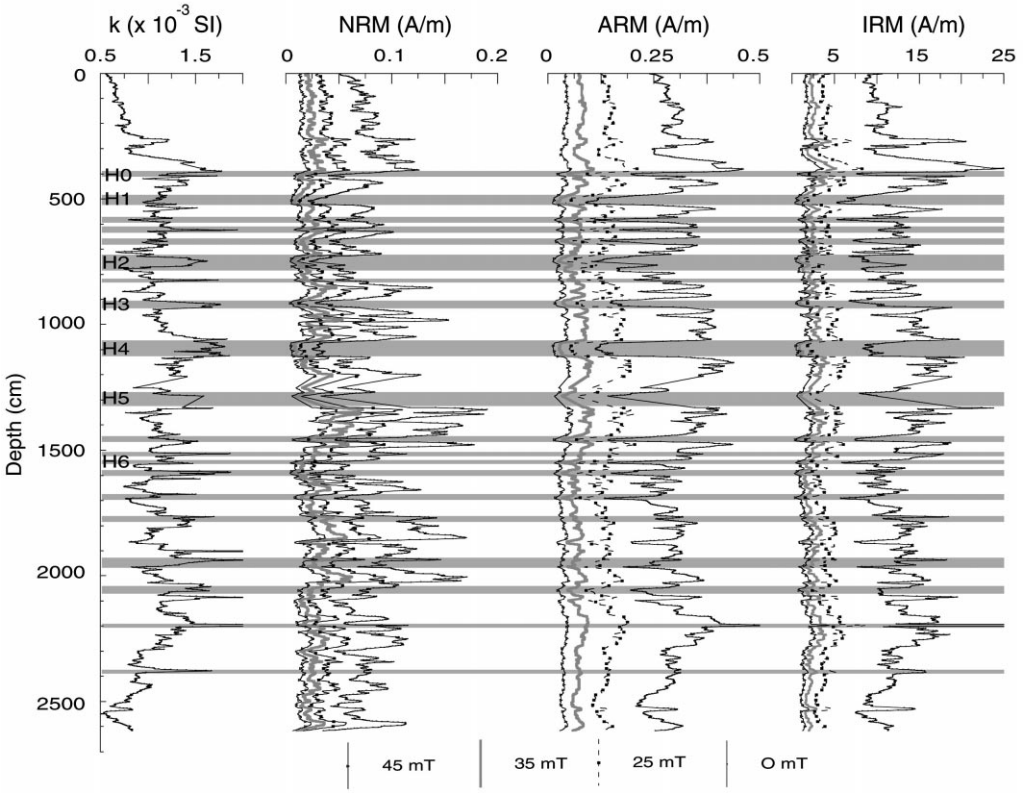

Fig. 2. Volumetric low field magnetic susceptibility (k) and the intensity of NRM, ARM and IRM after AF demagnetization at peak fields of 0, 25, 35 and 45 mT for u-channel samples from core MD95-2024. Shading represents detrital layers containing coarser (MD) magnetite and correlative to North Atlantic Heinrich (H) events as labeled (see [4]).

of remanence carrying grains [15]. These normalized NRM records provide proxies for relative variations in the strength of the geomagnetic field. A myriad of factors may affect the intensity of the NRM and therefore the paleointensity proxy. These include variations in magnetic and nonmagnetic mineralogy, sedimentation rate, environment of deposition, degree of bioturbation, diagenesis, compaction and coring or sampling induced disturbance. Separation of geomagnetic and environmental factors may be difficult, therefore, magnetic homogeneity has been considered a requirement for the development of trustworthy relative paleointensity records [16,17].

For core MD95-2024 sediments, we measured three potential normalizers: k, ARM and IRM. For efficient normalization, the coercivity of the normalizer should closely mimic that of the NRM [15]. The values of NRM/IRM are similar at different demagnetization levels, whereas for NRM/ARM, the ratio increases with increasing demagnetization level indicating that the NRM has a higher coercivity than the ARM. These data suggest that the IRM provides a better coercivity match (than ARM) to the NRM (**EPSL Online Background Dataset**, Fig. 2[1]).

Previous paleomagnetic studies from Labrador Sea sediments including sediments from this location (Core P-094) [3] have demonstrated that after removal of detrital layers, which contain coarse multidomain (MD) magnetite, these sediments pass the criteria for reliable paleointensity estimates [16,17]. Though the detrital layers are not strictly suitable for paleointensity determinations, they provide a detailed record of LIS instability that are traceable into the North Atlantic and therefore enhance the stratigraphic value of the core. The challenge is to develop a reliable paleo-

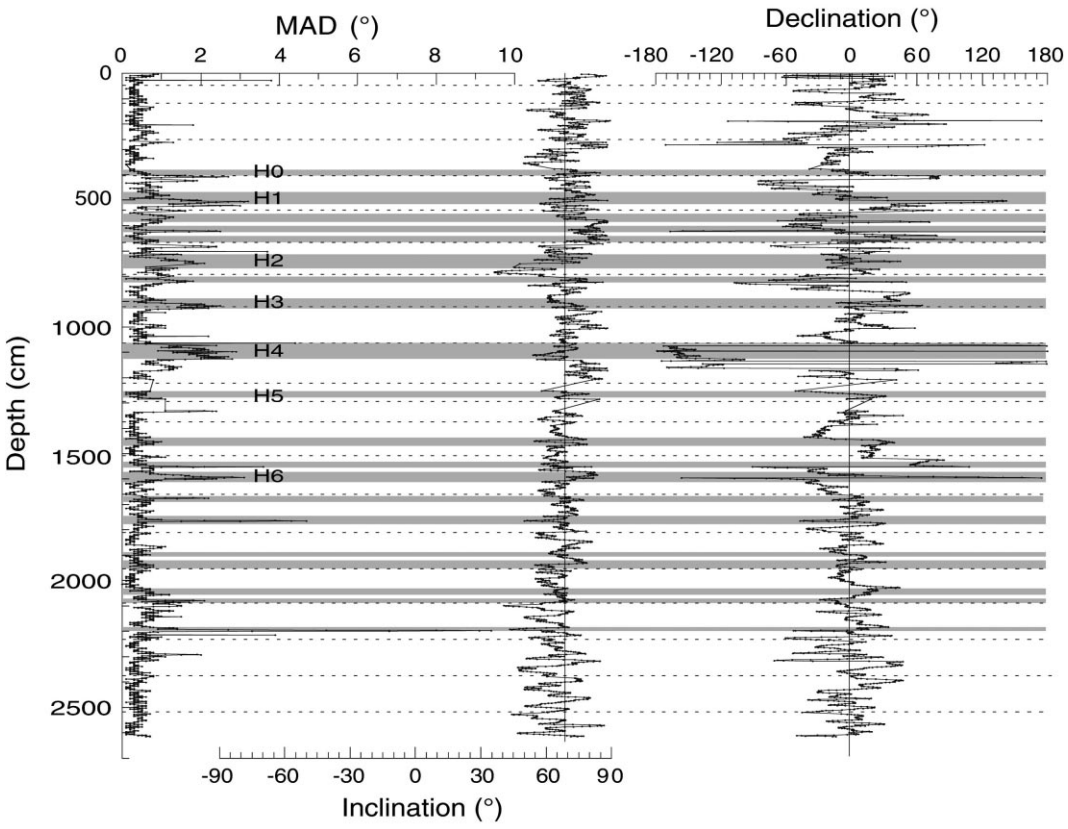

Fig. 3. Component declination and inclination and the associated MAD values calculated for AF demagnetization at peak demagnetization fields of 10, 25, 35 and 45 mT for core MD95-2024. The vertical line indicates expected inclination (67°) for site latitude. Coarse grained detrital layers are shaded, those correlative with North Atlantic Heinrich (H) events are labeled [4]. Dashed lines indicate core breaks.

intensity record without losing stratigraphic integrity.

Utilizing high-resolution magnetic hysteresis data collected from P-094 [3,10], we can estimate the value of k_{ARM}/k that corresponds to the subdivision of MD magnetite grains (not suitable for paleointensity) and pseudo-single-domain (PSD) grains (suitable for paleointensity) (**EPSL Online Background Dataset**, Fig. 3[1]). Based on the PSD to MD boundary determined from hysteresis data [18], the corresponding k_{ARM}/k cut-off value for core P-094 (>5 for PSD grains) is transferred to MD95-2024 on the basis of the k_{ARM}/k correlation of the two cores. Values of k_{ARM}/k of 5 in P-094 correspond to k_{ARM}/k of 3.5 in MD95-2024. The discrepancy may be attributed to the differing efficiency of ARM acquisition in u-channel (MD95-2024) and discrete samples (P-094). The shading shown in Figs. 2 and 3 correspond to the sediment where the k_{ARM}/k values are <3.5. Fig. 4 shows a plot of k_{ARM} versus k with different symbols indicating different grain size populations. Values of $k_{ARM}/k>5.5$ (rather than 3.5) represents a more restricted grain size cut-off, with the remaining data providing a uniform grain size for paleointensity determinations (Fig. 4).

With this reduced data set, restricted to $k_{ARM}/k>5.5$, four different paleointensity proxies were derived in order to minimize biases from any one method: $NRM_{25\,mT}/IRM_{25\,mT}$, $NRM_{25\,mT}/ARM_{25\,mT}$, $NRM_{25\,mT}-NRM_{35\,mT}/IRM_{25mT}-IRM_{35\,mT}$, and $NRM_{25\,mT}-NRM_{35\,mT}/ARM_{25\,mT}-ARM_{35\,mT}$. The paleointensity prox-

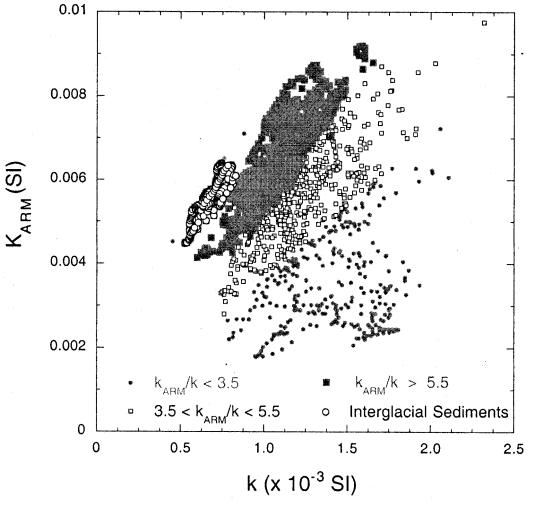

Fig. 4. k_{ARM} plotted against k for core MD95-2024. k_{ARM} = anhysteretic susceptibility, k = volume susceptibility.

ies were synchronized to a common low value at 1145 cm, then normalized by the mean value of each record and a four point running mean was calculated (Fig. 5a). This represents our most restrictive paleointensity proxy for these sediments, however, much of the stratigraphic continuity is lost. In Fig. 5b, we use the same four paleointensity proxies but no sediment is removed from the record. In Fig. 5c the arithmetic means, of the four paleointensity proxies shown in Fig. 5a,b, are calculated and the $\pm 1\sigma$ error estimates are shown. Very little difference is observed between the grain size restricted paleointensity proxy and that derived from the complete record (Fig. 5c), suggesting that a reliable record of geomagnetic field strength is preserved in these sediments, notwithstanding the heterogeneity in magnetite grain size. This surprising finding can be explained by

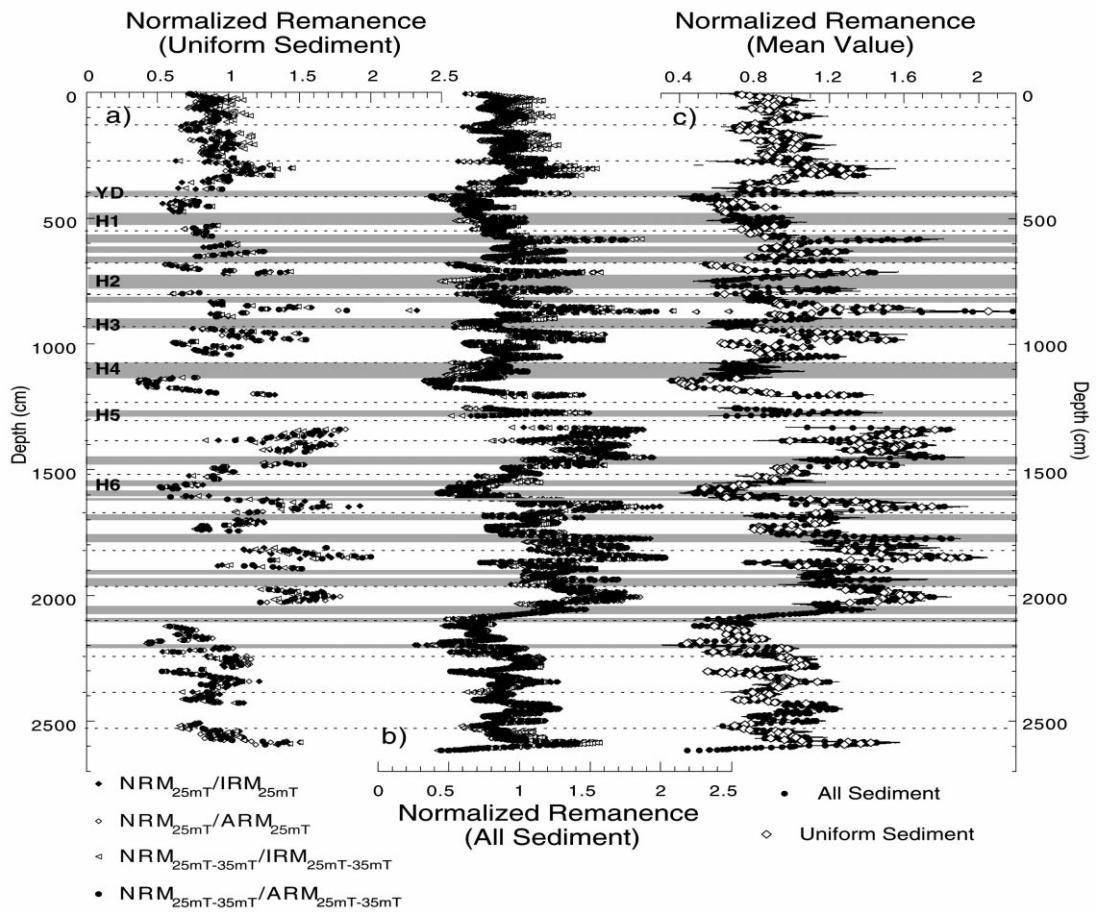

looking at a plot of ARM versus IRM (Fig. 6) which show that these are linearly related to each other. Comparison of Fig. 6 with Fig. 4 indicates that susceptibility (k) is picking up most of the grain size changes, while remanent magnetizations, ARM and IRM, are relatively insensitive to these changes (see **EPSL Online Background Dataset**[1] for the down-core IRM/ARM record, Fig. 4). The shading in Fig. 7 and in subsequent figures mark the position of the detrital layers containing MD magnetite as defined by $k_{ARM}/k < 3.5$. Although these layers do not appear to distort the paleointensity record, caution should be used with these intervals. In general, the u-channel paleointensity data for core MD95-2024 compare favorably with discrete sample data from the other Labrador Sea cores (P-094 and P-012 and P-013) [3,4] (**EPSL Online Background Dataset**, Fig. 1[1]).

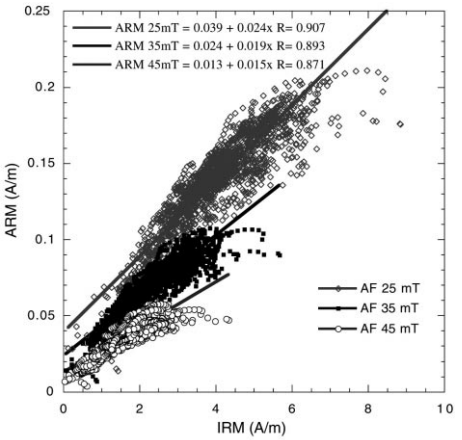

Fig. 6. ARM plotted against IRM after demagnetization at peak fields of 25, 35 and 45 mT for core MD95-2024.

4. Correlation of Labrador Sea sediments to Greenland ice cores

Remarkable climatic variations are preserved at millennial time scales in the Greenland Summit ice cores (GRIP/GISP2) [19,20]. Bond et al. [21] found that a North Atlantic sea surface temperature (SST) proxy mimics the pattern of rapid variations in air temperature proxies found in the Greenland Summit ice cores. Because these sediment cores contained Heinrich layers, by assuming that the SST and air temperature proxies were in phase, it became possible to transfer the stratigraphic position of the Heinrich layers to their equivalent position within the ice core. Based on similar logic this correlation was extended into isotopic stage 5 [22]. The development of a robust Labrador Sea chronostratigraphy and the assumed correlation of Labrador Sea detrital layers to North Atlantic Heinrich layers [4] provides a means of placing Labrador Sea sediments on a common temporal framework with the Greenland Summit ice cores (GRIP/GISP2) (Fig. 7). This is further constrained by the position of ash layer 2 found in both the Labrador Sea [4] and the GISP2 ice core [23].

The resulting ice core/sediment correlation is supported by the inverse match of the MD95-2024 paleointensity record to the flux of ^{36}Cl [24] and ^{10}Be [25] measured in the GRIP and GISP2 ice cores, respectively. Geomagnetic shielding as primary control on the long period flux of cosmic rays to the upper atmosphere has previously been demonstrated for ^{10}Be data from Vostok [26] and ^{36}Cl data in GRIP [24]. In Fig. 7, for the 30–90 ka interval, we have recalculated ^{36}Cl flux in the GRIP ice core using the GISP2 official chronology transferred to the GRIP ice core based on the correlation of the $\delta^{18}O_{ice}$ from the two cores. In the upper part of the record we splice in the ^{10}Be flux from the GISP2 ice core

←

Fig. 5. (a) NRM/ARM and NRM/IRM for sediment conforming to the uniform grain size criteria (based on the parameter k_{ARM}/k) after demagnetization at peak fields of 25 mT, and difference vector for NRM/ARM and NRM/IRM in the 25–35 mT demagnetization interval. (b) NRM/ARM and NRM/IRM for all sediment after demagnetization at peak fields of 25 mT, and difference vector for NRM/ARM and NRM/IRM in the 25–35 mT demagnetization interval. Legend the same as in (a). (c) The arithmetic means of the four paleointensity proxies, for all sediment (see b) (small closed circles) and for sediment conforming to the uniform grain size criteria (see a) (larger open diamonds). The $\pm 1\sigma$ error estimates are shown as horizontal lines. Coarse grained detrital layers are shaded, those correlative with North Atlantic Heinrich (H) events are labeled [4]. Dashed lines indicate section breaks.

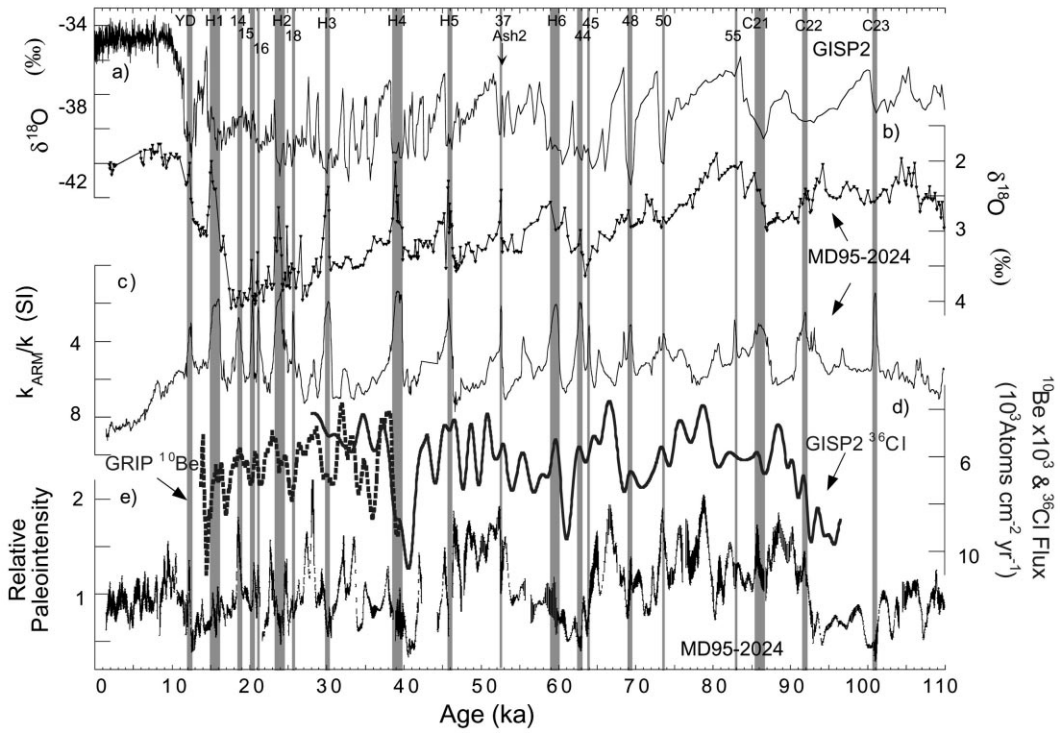

Fig. 7. Correlation of Labrador Sea sediment to Greenland Summit ice cores. (a) GISP2 $\delta^{18}O$ [20] placed on the GISP2 official chronology [31,32]. (b) The *N. pachyderma* (sin.) derived planktic $\delta^{18}O$ from core MD95-2024 [12] on a chronology resulting from (c). (c) k_{ARM}/k from core MD95-2024 correlated to GISP2 $\delta^{18}O$ by association of detrital layers (low values of k_{ARM}/k) to cold stadials (high values of $\delta^{18}O$). (d) ^{36}Cl flux in the GRIP ice core (from [24]) that was smoothed using a 3000 yr low pass filter placed on the GISP2 chronology [31,32]. ^{10}Be flux from the GISP2 ice core [25] smoothed with a five point running mean on the GISP2 official chronology [31,32]. (e) Geomagnetic paleointensity for Labrador Sea core MD95-2024 as in Fig. 5c. The chronology derived as in (c). Shading represents detrital layers containing coarser (MD) magnetite. YD = younger Dryas, H = numbered Heinrich events, C = numbered marine polar episodes (after [22]). Numbers correspond to numbered ~1500 yr cycle (after [48]). Vertical arrow indicates stratigraphic position of ash layer 2 [4,23].

[25] for the interval from 15–40 ka. Above this level environmental changes are too large to be accounted for by a simple flux calculation (see [25]) therefore these values are not used. The correlation between paleointensity records and cosmogenic isotopes observed here is consistent with those previously proposed [1,24,26]. Here we provide confirmation that high-frequency variations in geomagnetic field intensity also result in cosmogenic isotope flux changes [27] (Fig. 7).

Independently correlated to the GISP2 ice core, the NAPIS-75 paleointensity stack [1] comprises six relative paleointensity records from the North Atlantic distributed from 34°N to 68°N (Fig. 8). The chronology for NAPIS-75, during marine isotope stage (MIS) 3 [2], is based on the correlation of the planktic $\delta^{18}O$ record of core PS2644 [28] (one of the cores comprising the NAPIS stack) to the GISP2 $\delta^{18}O_{ice}$. Below MIS 3, the isotopic stage boundaries are used for age determinations. Correlation among the NAPIS cores was initially determined using isotopic stage boundaries with a second step matching magnetic susceptibility cycles [2]. These striking cycles are observed in locations strongly influenced by bottom current circulation within the Nordic Seas and the North Atlantic [2,29]. Kissel et al. [2] have established that these cycles are a response to reorganizations of the thermohaline circulation system and are coeval with the rapid temperature oscillations observed in the Greenland Summit ice cores during MIS 3. Placed on their independent age models,

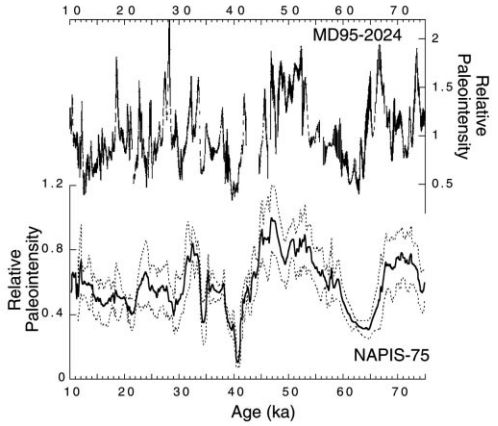

Fig. 8. Geomagnetic paleointensity for Labrador Sea core MD95-2024, time scale as in Fig. 7, compared with NAPIS-75 North Atlantic paleointensity stack [1] on its own time scale (see [2]). Stippled lines indicate ± 2σ incertitude derived from the bootstrap calculation.

the MD95-2024 paleointensity record compares favorably with NAPIS-75 (Fig. 8) indicating that both methods of marine to ice core correlation are compatible for the last 60 kyr. A chronological offset is, however, apparent at the paleointensity high at 65 ka and the subsequent low at 62 ka (Fig. 8). To see if the NAPIS-75 chronology could be modified without violating the linkage to the ice core, we adjusted the chronology of a single core within the NAPIS stack (MD95-2009) to better conform to that of MD95-2024. Fig. 9 illustrates that this can be accomplished without violating the linkage between magnetic susceptibility cycles and GISP2 $\delta^{18}O_{ice}$ record, while also improving the agreement between MD95-2009 paleointensity and the ice core cosmogenic isotope records.

5. Global correlation of paleointensity and cosmogenic isotope records

The observation of synchronous high-frequency (10^3 yr) variations in both the filter (proxy records of geomagnetic paleointensity) and the filtrate (cosmogenic isotope flux) suggests that these variations are due to global scale geomagnetic field changes (e.g. [1,26,24]). Using all available stratigraphic constraints we attempt to assess the validity of the assumption of global millennial scale variability of the paleointensity record. Fig. 10 shows ^{10}Be from GISP2 [25], ^{36}Cl from GRIP [24], the relative ^{10}Be flux from Vostok [26,30] and various high-resolution geomagnetic paleointensity records, all placed on the GISP2 official chronology [31,32]. The adjustment of the original

Table 1
Correlation coefficients (*r*)

Paleointensity cosmogenic isotope records	MD95-2024 paleointensity		GISP2 ice core	
	0–110 ka	20–110 ka	δ^{18}O gas 0–110 ka	δ^{18}O records
MD95-2024			0.655	MD95-2024
MD95-2009 (9–70 ka)	0.53	0.595		
Site 983	0.526	0.556	0.566	Site 983
Mediterranean (8–83 ka)	0.656	0.782	0.685	KET-8004
Somali Basin		0.687	0.8	Somali Basin
21-PC02	0.555	0.655	0.75	21-PC02
Sint200	0.289	0.576	0.888	SPECMAP
GRIP ^{36}Cl (28–96 ka)		0.581		
GISP2 ^{10}Be (15–40 ka)	0.523			
Vostok ^{10}Be	0.057	0.146	0.928	Vostok δ^{18}O gas

Chronology used to determine correlation coefficients the same as in Figs. 7, 9, 10 and 13. Correlation coefficients (*r*) calculated using Analyseries software [50]. Paleointensity records: MD95-2024 (this study), MD95-2009 [1], Site 983 [5], Mediterranean [6], Somali Basin [7], sub-Antarctic South Atlantic 21-PC02 [8], Sint-200 [9]. Cosmogenic isotope records: ^{36}Cl GRIP ice core [24], ^{10}Be GISP ice core [25], ^{10}Be Vostok ice core [26,30], δ^{18}O records: GISP2 [35], MD95-2024 *N. pachyderma* (sin.) [12], Site 983 *C. wuellerstorfi* [5], KET-8004 *G. bulloides* [43], Somali Basin bulk sediment [41], 21-PC02 *C. wuerllerstorfi* [8,42], SPECMAP [38], Vostok [35,40].

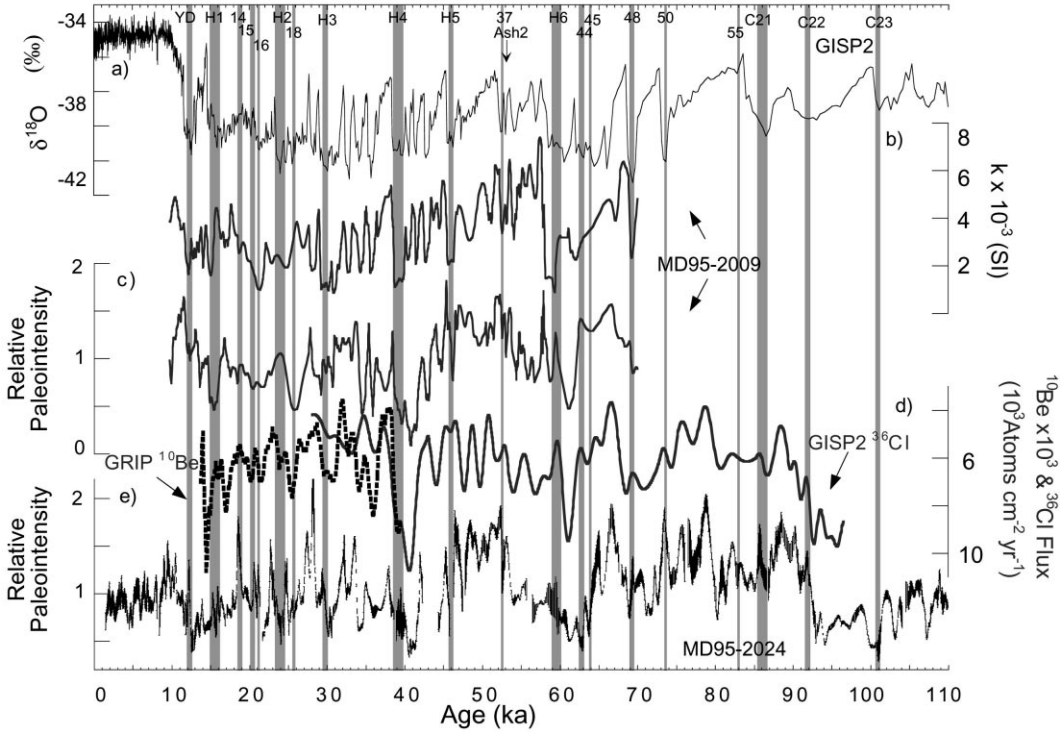

Fig. 9. Correlation of MD95-2009 to MD95-2024 and GISP2 ice core. (a) GISP2 $\delta^{18}O$ [20] placed on the GISP2 official chronology [31,32]. (b) Magnetic susceptibility (k) from core MD95-2009 [2]. The chronology for MD95-2009 is based on the Kissel et al. [2] chronology from 10–48 ka and is adjusted for ages >48 ka to derive a more pleasing match between the paleointensity records from MD95-2009 (d) and MD95-2024 (e). (c) ^{36}Cl flux in the GRIP ice core (from [24]) smoothed using a 3000 yr low pass filter placed on the GISP2 official chronology [31,32]. ^{10}Be flux from the GISP2 ice core [25] smoothed with a five point running mean and placed on the GISP2 official chronology [31,32]. (d) Geomagnetic paleointensity for Norwegian Sea core MD95-2009 [1]. The chronology for MD95-2009 is as stated above. (e) Geomagnetic paleointensity for Labrador Sea core MD95-2024. The chronology for MD95-2024 is as derived in Fig. 7. Shading represents stratigraphic position of detrital layers in MD95-2024 (see Fig. 7). YD = younger Dryas, H = numbered Heinrich events, C = numbered marine polar episodes (after [22]). Numbers correspond to numbered $\sim$1500 yr cycles (after [48]). Vertical arrow indicates stratigraphic position of ash layer 2 [2,4,23].

chronology of each record to the GISP2 official chronology is based on the following procedure: (1) synchronization of paleointensity lows and cosmogenic isotope spikes at $\sim$40 and $\sim$61 ka. (2) Synchronization of the Vostok δD_{ice} chronology to the GRIP $\delta^{18}O_{ice}$ chronology between 10 and 50 ka based on correlation of methane in trapped gas [33]. Note that the chronology for

→

Fig. 10. Geomagnetic paleointensity records and cosmogenic isotope records. All placed on the GISP2 official chronology. (a) ^{10}Be flux from the GISP2 ice core (latitude/longitude: 72°36N/38°30W) [25] and ^{36}Cl flux from the GRIP ice core (latitude/longitude: 72°34N/37°37W) [24]. Geomagnetic paleointensity records: (b) MD95-2024 (latitude/longitude: 50°12.N/45°41.W). (c) MD95-2009 (latitude/longitude: 62°44.N/3°59.W) [1]. (d) North Atlantic ODP Site 983 [5] (latitude/longitude: 60°24N/23°38.W). (e) Mediterranean stack [6] (latitude/longitude: 39°41N/13°35 E). (f) Somali Basin stack [7] (latitude/longitude: 1°0S/46°02 E). (g) Sub-Antarctic South Atlantic core 21-PC02 [8] (latitude/longitude: 41°08S/7°48E). (h) Relative ^{10}Be flux from the Vostok ice core [26,30] (latitude/longitude: 78°28S/106°48E). (i) Sint-200 global paleointensity composite [9]. Shading represents stratigraphic position of detrital layers in MD95-2024 (see Fig. 7). YD = younger Dryas, H = numbered Heinrich events, C = numbered marine polar episodes (after [22]). Numbers correspond to numbered $\sim$1500 yr cycles (after [48]). Vertical arrow indicates stratigraphic position of ash layer 2 [2,4,23].

GRIP has been adjusted to conform to the GISP2 official chronology [31,32] from the original chronology [34] used by Blunier et al. [33]. This synchronization is consistent with the synchroneity of the cosmogenic isotope spike at ~40 ka. (3) For the older part of our Vostok chronology we have linearly interpolated between tie points based on $\delta^{18}O_{gas}$ in GISP2 and Vostok [35]. To derive the

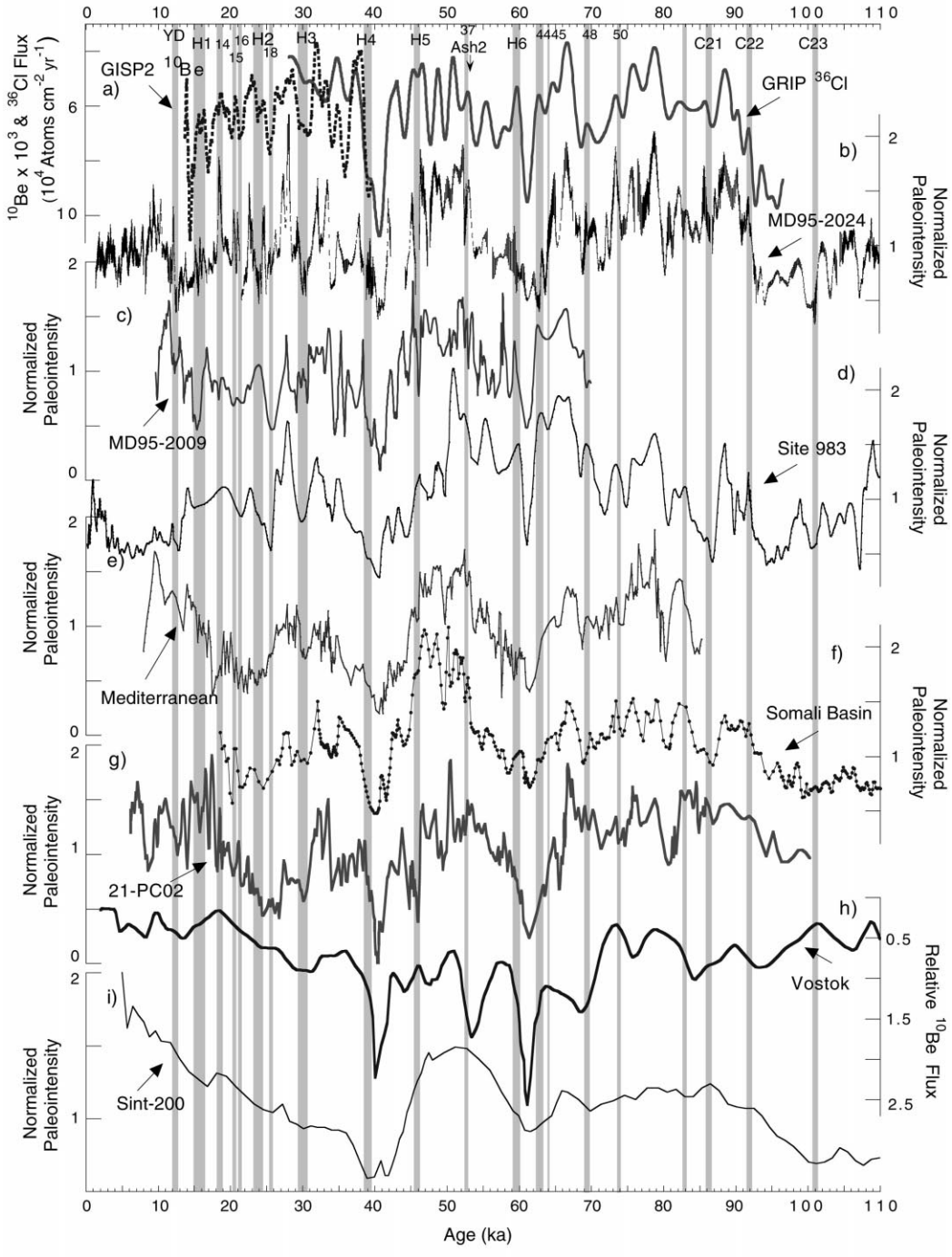

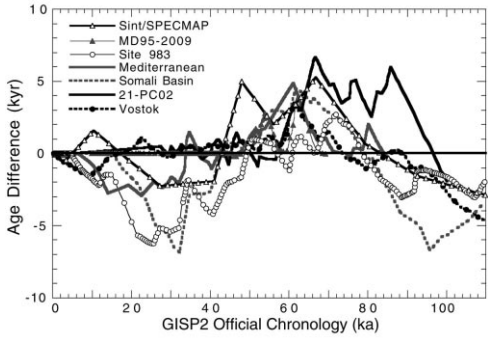

Fig. 11. Age differences between published age models and GISP2 chronostratigraphy (this paper) versus the GISP2 official chronology [31,32]: ODP Site 983 [5], core 21-PC03 [8], Mediterranean stack [6,43]; Somali Basin stack [7,41]; SPECMAP [38]; Sint-200 [9] and Vostok ice core [42]. Positive (negative) age differences indicate that the original published age models are older (younger) than the GISP2 age.

δD_{ice} age, we used the Petit et al. [36] continuous Δages (gas age−ice age difference) based on the model of Barnola et al. [37]. (4) Based on our assumption that the paleointensity record from MD95-2024 (placed on the GISP2 chronology) is representative of global geomagnetic field variability, the chronologies of the other paleointensity records are adjusted to achieve optimal correlation (Table 1). The resulting GISP2 chronology yields age offsets up to $\sim$5 kyr relative to the original (published) chronologies for each record similar to the offset reported in [1] (Fig. 11). This age offset is within the stated uncertainty of SPECMAP time scale [38] but slightly larger than the stated uncertainties within the GISP2 official chronology (see [31,32]).

6. A new global chronostratigraphy

An initial test of the validity of the paleointensity correlation shown in Fig. 10 is provided by correlation of the 'global' component of the associated $\delta^{18}O$ records (Fig. 12). The stacking procedure used to derive the Sint-200 paleointensity stack [9] was based on re-correlation of each associated $\delta^{18}O$ record to the SPECMAP $\delta^{18}O$ stack [38]. Therefore, the adjustment of the Sint-200 time scale to the GISP2 official chronology based on paleointensity constraints (Fig. 10), must be balanced by an equivalent adjustment of the time scale of the SPECMAP $\delta^{18}O$ record (Fig. 12). If $\delta^{18}O_{gas}$ in GISP2 and Vostok reflects changes in mean $\delta^{18}O$ of the ocean [35,39,40], then the chronostratigraphic adjustments made to Sint-200 (Fig. 10) and by association SPECMAP (Fig. 12), should result in a satisfying correlation of the SPECMAP $\delta^{18}O$ record to the $\delta^{18}O_{gas}$ records from GISP2 and Vostok, as well as the associated benthic $\delta^{18}O$ records (Fig. 12), also placed on a GISP2 chronology. It should be noted that the correlation between GISP2 $\delta^{18}O_{gas}$ and SPECMAP $\delta^{18}O$ is improved using the new chronology (from $r = 0.855$ to 0.888). In general the match is very good, especially for $\delta^{18}O_{gas}$ in GISP2, the bulk sediment $\delta^{18}O$ from the Somali Basin [41] and the benthic $\delta^{18}O$ record of 21-PC02 [8,42] (Fig. 12) (Table 1). Slightly poorer correlation is found for the Vostok $\delta^{18}O_{gas}$ record (Fig. 12), which may result from the large uncertainty in Δage of this low accumulation rate ice core [36,37]. Discrepancies from the global signal are observed in Labrador Sea core MD95-2024, Mediterranean core KET-8004 [43], and North Atlantic ODP Site 983 [5] (Fig. 12). The first two are planktic records where local deviations are to be expected. The Site 983 isotope record is a benthic record and, therefore, these deviations, which are similar to those in the MD95-2024 planktic record (Fig. 12), may result from local millennial scale variability penetrating to intermediate water depths (1983 m) at this location.

Fig. 13 illustrates that distinct regional patterns in millennial scale climate are also preserved within this chronostratigraphy. Charles et al. [44] argued that within sediment cores from the sub-Antarctic South Atlantic, the planktic ($\delta^{18}O$) and benthic ($\delta^{13}C$) isotopes provide proxy records of millennial scale climate characteristic of the southern and northern hemispheres, respectively. Benthic $\delta^{13}C$ was interpreted to reflect changes in the flux of North Atlantic deep water which are in phase with warming in Greenland, while planktic $\delta^{18}O$ was interpreted to represent changes in SSTs and that warming of the sub-Antarctic South Atlantic leads that observed in the Greenland Summit ice cores by approximately 1500 yr [43,42].

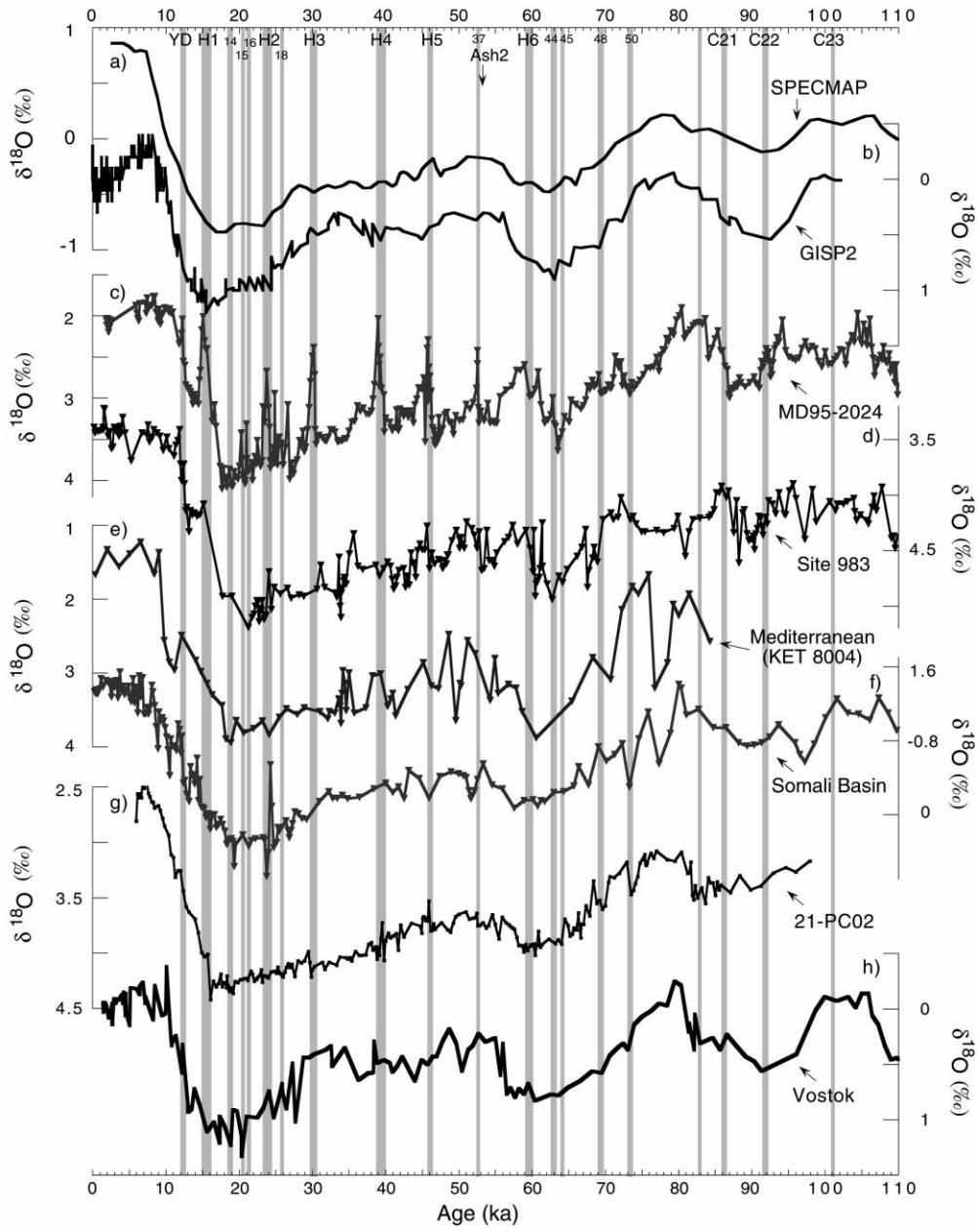

Fig. 12. Ice core and marine isotope records on a common GISP2 age model. (a) SPECMAP $\delta^{18}O$ [38]. (b) $\delta^{18}O_{gas}$ from the GISP2 ice core [35]. (c) Labrador Sea MD95-2024 planktic $\delta^{18}O$ from *N. pachyderma* (sin.) [12]. (d) North Atlantic ODP Site 983 benthic $\delta^{18}O$ from *Cibicidoides wuellerstorfi* [5]. (e) Mediterranean core KET 8004 planktic $\delta^{18}O$ from *Globigerina bulloides* [43]. (f) Somali Basin bulk sediment $\delta^{18}O$ [41]. (g) Sub-Antarctic South Atlantic core 21-PC02 benthic $\delta^{18}O$ from *C. wuellerstorfi* [8,42]. (h) $\delta^{18}O_{gas}$ from the Vostok ice core [5,40]. Shading represents stratigraphic position of detrital layers in MD95-2024 (see Fig. 7). YD = younger Dryas, H = numbered Heinrich events, C = numbered marine polar episodes (after [22]). Numbers correspond to numbered ~1500 yr cycles (after [48]). Vertical arrow indicates stratigraphic position of ash layer 2 [2,4,23].

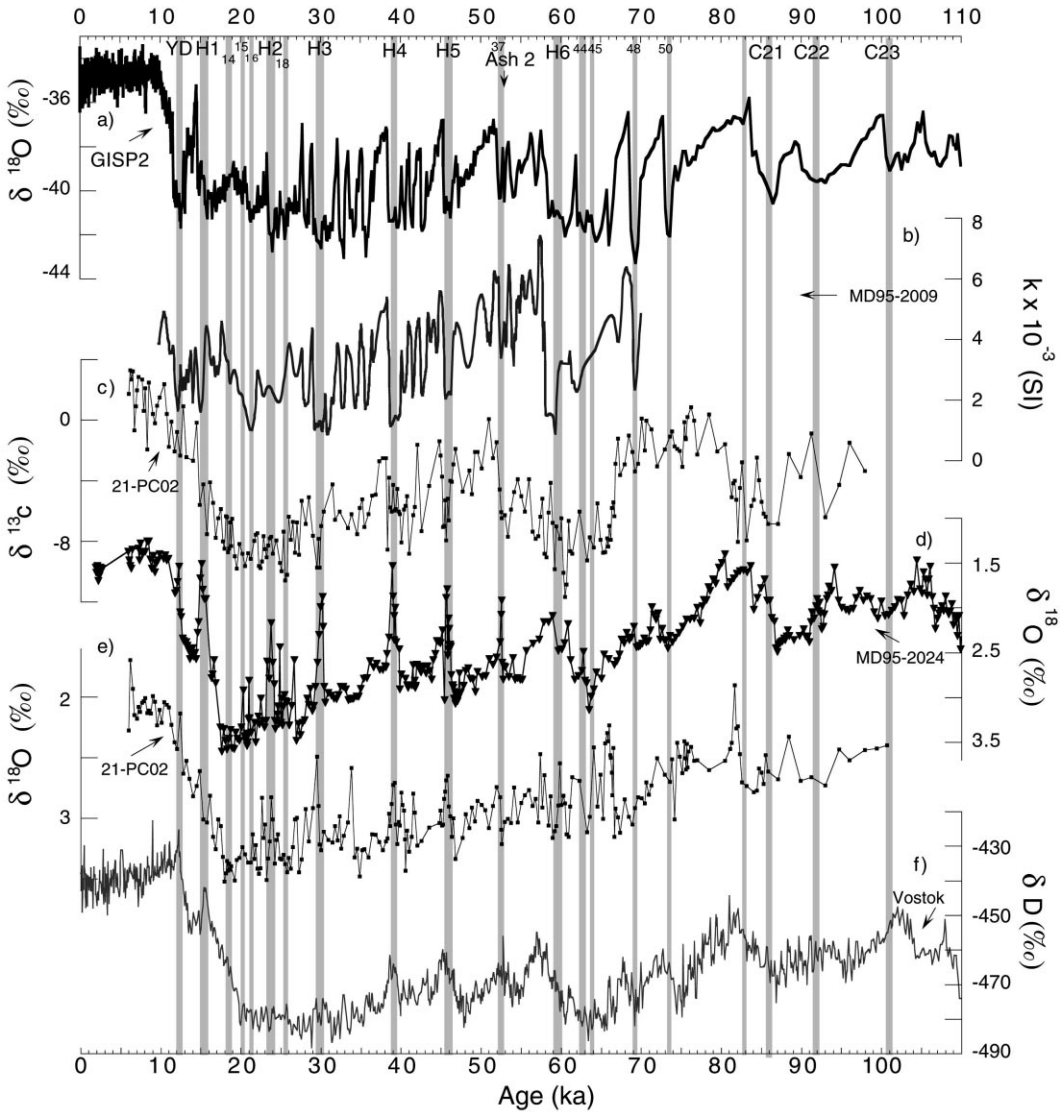

Fig. 13. Ice core and marine isotope records on a common GISP2 age model. (a) GISP2 $\delta^{18}O$ [20]. (b) Norwegian Sea core MD95-2009 magnetic susceptibility data [2]. (c) Sub-Antarctic South Atlantic core 21-PC02 benthic $\delta^{13}C$ from *C. wuellerstorfi* [8,42]. (d) Labrador Sea MD95-2024 planktic $\delta^{18}O$ from *N. pachyderma* (sin.) [12]. (e) Sub-Antarctic South Atlantic core 21-PC02 planktic $\delta^{18}O$ from *G. bulloides* [8,42]. (f) Vostok δD [49]. Shading represents stratigraphic position of detrital layers in MD95-2024 (see Fig. 7). YD = younger Dryas, H = numbered Heinrich events, C = numbered marine polar episodes (after [22]). Numbers correspond to numbered ~1500 yr cycles (after [48]). Vertical arrow indicates stratigraphic position of ash layer 2 [2,4,23].

This apparent out of phase behavior between the northern and southern hemispheres has been found in several subsequent studies in marine sediments [45,46] and ice cores [33], and has been inferred from modeling results (e.g. [47]). The chronostratigraphy in Fig. 13 preserves this relationship for sub-Antarctic South Atlantic core 21-PC02. In addition, LIS instability, recorded in MD95-2024 by planktic $\delta^{18}O$ spikes denoting meltwater dilution and by k_{ARM}/k denoting dis-

tinct detrital layers, is synchronous with warming in the sub-Antarctic South Atlantic and at Vostok (Fig. 13). This supports the linkage between fresh water flux to the North Atlantic, thermohaline circulation change, cooling of North Atlantic regions air temperature and SSTs and warming of sub-Antarctic South Atlantic SSTs and the air over Vostok. Because we are able to pull out an expected, but not independently demonstrated, global chain of events strongly supports the merits of this stratigraphy. Based on these results, we suggest that all records are on a common temporal framework that is tied to the GISP2 official chronology. We want to make clear that the age adjustment of SPECMAP is a stratigraphic adjustment and not an indication that the SPECMAP chronology is necessarily incorrect. However, it does appear that there are clear discrepancies between GISP2 and SPECMAP (Fig. 12) even in the interval where they are supposedly synchronized [32].

Fig. 10 demonstrates that the time scale of variability of global scale geomagnetic field is less than a few thousand years, and that these high-frequency changes are reflected in the flux of cosmogenic isotopes recorded in ice cores. Even though there is a strong global similarity for the various paleointensity records, amplitude differences are commonly observed among correlative features (Fig. 10). Some of these amplitude changes may be regional, however, too few records exist to determine if these are geomagnetic or environmental in origin. Because the high-resolution paleointensity records are derived from sediments that show both in-phase and out-of-phase climate relationships at millennial and orbital scales, the synchronization of the paleointensity records cannot be a product of climate variability.

Acknowledgements

We thank Guy Bilodeau for u-channel sampling and logistics, J. Beer, C. Charles, Y. Guyodo, D. Hodell and A. Mazaud for providing digital data, and T. Yamazaki for reviewing the manuscript. We would also like to acknowledge the IMAGES program and the IFRTP for core collection. Research supported provided by US National Science Foundation grant INT 95-12821 through the France-US collaborative science program. This is LSCE contribution No. 0494.*[RV]*

References

[1] C. Laj, C. Kissel, A. Mazaud, J.E.T. Channell, J. Beer, North Atlantic paleointensity stack since 75 ka (NAPIS-75) and the duration of the Laschamp event, Philos. Trans. R. Soc. Ser. A 358 (2000) 1009–1025.

[2] C. Kissel, C. Laj, L. Labeyrie, T. Dokken, A. Voelker, D. Blamart, Rapid climatic variations during marine isotope stage 3: magnetic analysis of sediments from Nordic Seas and North Atlantic, Earth Planet. Sci. Lett. 171 (1999) 489–502.

[3] J.S. Stoner, J.E.T. Channell, C. Hillaire-Marcel, Late Pleistocene relative geomagnetic paleointensity from the deep Labrador Sea: regional and global correlations, Earth Planet. Sci. Lett. 134 (1995) 237–252.

[4] J.S. Stoner, J.E.T. Channell, C. Hillaire-Marcel, A 200 kyr geomagnetic stratigraphy for the Labrador Sea: indirect correlation of the sediment record to SPECMAP, Earth Planet. Sci. Lett. 159 (1998) 165–181.

[5] J.E.T. Channell, D.A. Hodell, B. Lehman, Relative paleointensity and $\delta^{18}O$ at ODP Site 983, since 350 ka, Earth Planet. Sci. Lett. 153 (1997) 103–118.

[6] E. Tric, J.-P. Valet, P. Tucholka, M. Paterne, L. Labeyrie, F. Guichard, L. Tauxe, M. Fontugne, Paleointensity of the geomagnetic field during the last 80 000 years, J. Geophys. Res. 97 (1992) 9337–9351.

[7] L. Meynadier, J.-P. Valet, R. Weeks, N.J. Shackleton, V.L. Hagee, Relative geomagnetic intensity of the field during the last 140 ka, Earth Planet. Sci. Lett. 114 (1992) 39–57.

[8] J.E.T. Channell, J.S. Stoner, D.A. Hodell, C. Charles, Geomagnetic paleointensity from late Brunhes-age piston cores from the subantarctic South Atlantic, Earth Planet. Sci. Lett. 175 (2000) 145–160.

[9] Y. Guyodo, J.P. Valet, Relative variations in geomagnetic intensity from sedimentary records: the past 200 000 years, Earth Planet. Sci. Lett. 143 (1996) 23–46.

[10] J.S. Stoner, J.E.T. Channell, C. Hillaire-Marcel, The magnetic signature of rapidly deposited detrital layers from the deep Labrador Sea: relationship to North Atlantic Heinrich layers, Paleoceanography 11 (1996) 309–325.

[11] C. Hillaire-Marcel, A. de Vernal, G. Bilodeau, G. Wu, Isotope stratigraphy, sedimentation rates, deep circulation and carbonate events in the Labrador Sea during the last $\sim$200 ka, Can. J. Earth Sci. 31 (1994) 63–89.

[12] C. Hillaire-Marcel, G. Bilodeau, Instabilities in the Labrador Sea water mass structure during the last climatic cycle, Can. J. Earth Sci. 37 (2000) 795–809.

[13] R.J. Weeks, C. Laj, L. Endignoux, M.D. Fuller, A.P. Roberts, R. Manganne, E. Blanchard, W. Goree, Improvements in long core measurement techniques: applications in palaeomagnetism and palaeoceanography, Geophys. J. Int. 114 (1993) 651–662.
[14] J.L. Kirschvink, The least squares lines and plane analysis of paleomagnetic data, Geophys. J. R. Astrol. Soc. 62 (1980) 699–718.
[15] S. Levi, S.K. Banerjee, On the possibility of obtaining relative paleointensities from lake sediments, Earth Planet. Sci. Lett. 29 (1976) 219–226.
[16] J.W. King, S.K. Banerjee, J. Marvin, A new rock magnetic approach to selecting sediments for geomagnetic intensity studies: application to paleointensity for the last 4000 years, J. Geophys. Res. 88 (1983) 5911–5921.
[17] L. Tauxe, Sedimentary records of relative paleointensity of the geomagnetic field: theory and practice, Rev. Geophys. 31 (1993) 319–354.
[18] R. Day, M. Fuller, V.A. Schmidt, Hysteresis properties of titanomagnetites: grain-size and compositional dependence, Phys. Earth Planet. Inter. 13 (1977) 260–267.
[19] W. Dansgaard, S.J. Johnsen, H.B. Clausen, D. Dahl-Jensen, N.S. Gundestrup, C.U. Hammer, C.S. Hvidberg, J.P. Steffensen, A.E. Sveinbjirnsdottir, J. Jouzel, G. Bond, Evidence for general instability of past climate from a 250-kyr ice-core record, Nature 364 (1993) 218–220.
[20] P.M. Grootes, M. Stuvier, Oxygen 18/16 variability in Greenland snow and ice with 10^{-3} to 10^{5}-year time resolution, J. Geophys. Res. 102 (1997) 26,455–26,470.
[21] G. Bond, W. Broecker, S. Johnsen, J. McManus, L. Labeyrie, J. Jouzel, G. Bonani, Correlations between climate records from North Atlantic sediments and Greenland ice, Nature 365 (1993) 143–147.
[22] J.F. McManus, G.C. Bond, W.S. Broecker, S. Johnsen, L. Labeyrie, S. Higgins, High-resolution climate records from the North Atlantic during the last interglacial, Nature 371 (1994) 326–329.
[23] G.A. Zielinski, P.A. Mayewski, L.D. Meeker, K. Grönvold, M.S. Germani, S. Whitlow, M.S. Twickler, K. Taylor, Volcanic aersosol records and tephrochronology of the Summit, Greenland, ice cores, J. Geophys. Res. 102 (1997) 26,625–26,640.
[24] S. Baumgartner, J. Beer, J. Masarik, G. Wagner, L. Meynadier, H.-A. Synal, Geomagnetic modulation of the ^{36}Cl flux in the GRIP ice Core, Greenland, Science 279 (1998) 1330–1332.
[25] R.C. Finkel, K. Nishiizumi, Beryllium 10 concentrations in the Greenland Ice Sheet Project 2 ice core from 3–40 ka, J. Geophys. Res. 102 (1997) 26699–26706.
[26] A. Mazaud, C. Laj, M. Bender, A geomagnetic chronology for antarctic ice accumulation, Geophys. Res. Lett. 21 (1994) 337–340.
[27] G. Wagner, J. Beer, C. Laj, C. Kissel, J. Mazarik, R. Muscheler, H.-A. Synal, Chlorine-36 evidence for the Mono Lake event in the Summit GRIP ice core, Earth Planet. Sci. Lett. 181 (2000) 1–6.
[28] A. Voelker, M. Sarnthein, P.M. Grootes, H. Erlenkeuser, C. Laj, A. Mazaud, M.J. Nadeau, M. Schleicher, Correlation of marine ^{14}C ages from the Nordic Sea with GISP2 isotope record: implication for ^{14}C calibration beyond 25 ka BP, Radiocarbon 40 (1998) 517–534.
[29] T.L. Rasmussen, E. Thompsen, T.C.E. Van Weering, L. Labeyrie, Rapid chages in surface and deep water conditions at the Faeroe margin during the last 58 000 years, Paleoceanography 11 (1996) 757–771.
[30] G.M. Raisbeck, F. Yiou, D. Bourles, C. Lorius, J. Jouzel, N.I. Barkov, Evidence for two intervals of enhanced ^{10}Be deposition in Antarctic ice during the last glacial period, Nature 326 (1987) 273–277.
[31] D.A. Meese, R.B. Alley, A.J. Gow. P.M. Grootes, P.A. Mayewski, M. Ram, K.C. Taylor, I.E. Waddington, G.A. Zielinski. Preliminary depth-age scale for the GISP2 ice core, Spec. Rep. 94-1, Cold Reg. Res. Eng. Lab., Hanover, NH, 1994.
[32] M.B. Bender, T. Sowers, M.-L. Dickson, J. Orchardo, P. Grootes, P.A. Mayewski, D.A. Messe, Climate correlations between Greenland and Antarctica during the past 100 000 years, Nature 372 (1994) 663–666.
[33] T. Blunier, J. Chappellaz, J. Schwander, A. Döllenbach, B. Stauffer, T. Stocker, D. Raynaud, J. Jouzel, H.B. Clausen, C.U. Hammer, S.J. Johnsen, Asynchrony of Antarctic and Greenland climate change during the last glacial period, Nature 394 (1998) 739–743.
[34] S. Johnsen, D. Dahl-Jensen, W. Dansgaard, N. Gundestrup, Greenland palaeotemperatures derived from GRIP bore hole temperature and ice core isotope profiles, Tellus 47B (1995) 624–629.
[35] M.B. Bender, B. Malaize, J. Orchardo, T. Sowers, J. Jouzel, High precision correlations of Greenland and Antarctic ice core records over the last 100 kyr, in: P.U. Clark, R.S. Webb, L.D. Keigwin (Eds.), Mechanisms of Global Climate Change at Millennial Time Scales, AGU, Washington, DC, 1999, pp. 149–164.
[36] J.R. Petit, J. Jouzel, D. Raynaud, N.I. Barkov, J.M. Barnola, I. Basile, M. Bender, J. Chappellaz, J. Davis, G. Delaygue, M. Delmotte, V.M. Kotlyakov, M. Legrand, V.M. Lipenkov, C. Lorius, L. Pépin, C. Ritz, E. Saltzman, M. Stievenard, Climate and atmospheric history of the past 420 000 years from the Vostok ice core, Antarctica, Nature 399 (1999) 429–436.
[37] J.M. Barnola, P. Pimienta, D. Raynaud, Y.S. Korotkevich, CO_2 climate relationship as deduced from the Vostok ice core: a re-examination based on new measurements and on a re-evaluation of the air dating, Tellus 43B (1991) 83–91.
[38] D.G. Martinson, N.G. Pisias, J.D. Hays, J. Imbrie, T.C. Moore Jr., N.J. Shackleton, Age dating and the orbital theory of the Ice Ages: development of a high-resolution 0 to 300 000-year chronostratigraphy, Quat. Res. 27 (1987) 1–29.
[39] T. Sowers, M. Bender, D. Raynaud, Y.S. Korotkevich, The δ^{18}O of atmospheric O_2 from air inclusions in the Vostok ice core: timing of CO_2 and ice volume changes

during the penultimate deglaciation, Paleoceanography 6 (1991) 679–696.
[40] T. Sowers, M. Bender, L. Labeyrie, D. Martinson, J. Jouzel, D. Raynaud, J.J. Pichon, Y.S. Korotkevich, A 135 000-year Vostok-SPECMAP common temporal framework, Paleoceanography 8 (1993) 737–766.
[41] N.J. Shackleton, M.A. Hall, D. Pate, L. Meynadier, P. Valet, High-resolution stable isotope stratigraphy from bulk sediment, Paleoceanography 8 (1992) 141–148.
[42] U.S. Ninnemann, C.D. Charles, D.A. Hodell, Origin of global millennial scale climate events: constraints from the Southern Ocean deep sea sedimentary record, in: P.U. Clark, R.S. Webb, L.D. Keigwin (Eds.), Mechanisms of Global Climate Change at Millennial Time Scales, AGU, Washington, DC, 1999, pp. 99–112.
[43] M. Paterne, F. Guichard, J. Labeyrie, P.Y. Gillot, J.C. Duplessy, Tyrrhenian sea tephrochronology of the oxygen isotope records for the past 60 000 years, Mar. Geol. 72 (1986) 259–285.
[44] C.D. Charles, J. Lynch-Stieglitz, U.S. Ninnemann, R.G. Fairbanks, Climate connections between the hemispheres revealed by deep sea sediment core/ice core correlations, Earth Planet. Sci. Lett. 142 (1996) 19–28.
[45] M.G. Little, R.R. Schneider, D. Kroon, B. Price, C.P. Summerhayes, M. Segl, Trade wind forcing of upwelling seasonality and Heinrich events as a response to sub-Milankovitch climate variability, Paleoceanography 12 (1997) 568–576.
[46] L. Vidal, R.R. Schneider, O. Marchal, T. Bickert, T.F. Stocker, G. Wefer, Link between the North and South Atlantic during the Heinrich events of the last glacial period, Clim. Dyn. 15 (1999) 909–919.
[47] A. Schiller, U. Mikolajewicz, R. Voss, The stability of the North Atlantic thermohaline circulation in a coupled ocean-atmosphere general circulation model, Clim. Dyn. 13 (1997) 324–347.
[48] G.C. Bond, W. Showers, M. Elliot, M. Evans, R. Lotti, I. Hajdas, G. Bonani, S. Johnson. The North Atlantic's 1–2 kyr climate rhythm: relation to Heinrich events, Dansgaard/Oeschger cycles and the little Ice Age, in: P.U. Clark, R.S. Webb, L.D. Keigwin (Eds.), Mechanisms of Global Climate Change at Millennial Time Scales, AGU, Washington, DC, 1999, pp. 35–58.
[49] J. Jouzel, C. Lorius, J.R. Petit, C. Genthon, N.I. Barkov, V.M. Kotlyakov, V.M. Petrov, Vostok ice core a continuous isotope temperature record over the last climatic cycle (160 000 years), Nature 329 (1987) 402–408.
[50] D. Paillard, L. Labeyrie, P. Yiou, Macintosh program performs time-series analysis, Eos Trans. AGU 77 (1996) 379.